Signatures of Fano resonances in four-wave-mixing experiments

T. Meier, A. Schulze, P. Thomas, and H. Vaupel
Department of Physics and Materials Sciences Center, Philipps University, D-35032 Marburg, Federal Republic of Germany

K. Maschke
Institut de Physique Appliquée, Ecole Polytechnique Fédérale de Lausanne, CH-1015 Lausanne, Switzerland
(Received 5 December 1994)

Optical transitions into discrete levels coupled to an optically active continuum lead to asymmetrical Fano lines in the linear absorption spectra, reflecting interference between the excitation channels. We investigate the corresponding four-wave-mixing spectra for the nonlinear optical response within a model of noninteracting electrons. Our results show that four-wave-mixing experiments provide a useful tool to identify Fano resonances.

I. INTRODUCTION

Asymmetrical Fano line shapes and antiresonances in the linear optical spectra (LS) result if an optical transition from a given ground state $|g\rangle$ into a state $|a\rangle$ is energetically degenerate with transitions from $|g\rangle$ into a continuum $|\tilde{E}_i\rangle$ of states, and if the state $|a\rangle$ is quantum mechanically coupled to the continuum $|\tilde{E}_i\rangle$ by some interaction $v_{E_i a}$, see Fig. 1(a). The asymmetry is a consequence of interference between the excitation of the discrete state and that of the continuum due to the coupling $v_{E_i a}$. In addition to that, the Fano situation requires that both the discrete level and the continuum are optically coupled to a common ground state. Fano line shapes are found in many areas of spectroscopy. For semiconductors, different situations have been discussed including magnetoexcitons in bulk semiconductors,[1] semiconductor heterostructures,[2–5] shallow quantum wells in an external electric field,[6] doped semiconductors,[7] and biexciton resonances.[8] Asymmetrical absorption lines and antiresonances have been observed in some of these cases[1]. Fano situations have also been discussed in relation with Raman scattering.[9]

The existence of an asymmetrical optical-absorption line alone, however, is not sufficient to prove the existence of a Fano interference. For example, excitonic absorption lines in semiconductors are not symmetrical. The lowest $1s$-excitonic line of a direct semiconductor has an exponential shape at the low-energy side, while it is Lorentzian at the high-energy side.[10] Asymmetrical shapes of the absorption spectrum may also be produced simply by overlapping resonances without mutual coupling. It would therefore be useful to find less ambiguous criteria for the existence of Fano resonances. Experimental investigations of the temporal dynamics are quite promising in this respect, because they may give direct evidence for the interference processes which are at the origin of these resonances. This is the basic idea of the present paper, in which we look for signatures of Fano interference in transient optical experiments.

It is evident that the importance of interference scales with the coupling $v_{E_i a}$. For vanishing $v_{E_i a}$ the linear spectrum is given by the superposition of a spectral line $|g\rangle \rightarrow |a\rangle$ and the spectrum of the continuum. The fact that the ground state is common to both sets of transitions is of no relevance to the linear spectrum in this particular case. On the other hand, this internal coupling of optical transitions by a common state can be observed

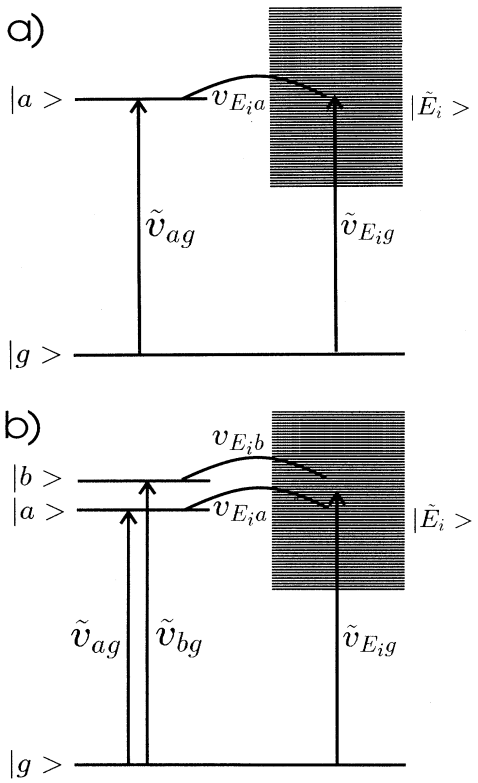

FIG. 1. Pictorial representation of the Hamiltonian for (a) $N = 1$, and (b) $N = 2$.

in nonlinear optics. For example, transient four-wave mixing spectroscopy is widely used to identify the dynamics of coupled optical transitions, for which quantum beats are the most prominent example (see references in Ref. 11).

Quantum beats occur if short laser pulses coherently excite two discrete optical resonances with frequency difference $\Delta\omega$ having one level in common, thus forming a three-level system. As mentioned above, the coupling of optical transitions due to the common state does not show up in linear spectra as a special feature. Two completely independent transitions, i.e., a pair of two-level systems having the same resonance frequencies as the three-level system, show exactly the same linear spectrum. Four-wave-mixing spectroscopy in the time domain, on the other hand, reveals the coupling due to a common state by showing beats in both the time-resolved (TR) and time-integrated (TI) mode with a particular signature in the t-τ plane[11] differing from that of two independent systems. Different quantum beat situations have been discussed in the literature, as $1s - 2s$ excitonic beats,[12] heavy-hole–light-hole excitonic beats,[13] beats from excitonic wave packets formed from the discrete and part of the continuous spectrum,[14] and beats resulting from optical excitation of eigenstates in two resonantly coupled quantum wells[15]. Beats with period $2\pi/\Delta\omega$ are observed in both the TR-trace and the TI-trace. Both the linear spectrum (LS) and the four-wave-mixing spectrum (FWMS) then show peaks separated by $\Delta\omega$.

We now turn to the Fano situation. In addition to the coupling via the common ground state, the quantum coherent dynamics of the excited states is due to the coupling $v_{E_i a}$ between $|a\rangle$ and the continuum states $|\tilde{E}_i\rangle$. An excitation initially prepared in $|a\rangle$ would decay exponentially into the continuum. However, since the continuum is simultaneously excited, the decay is modified by interference. A related interesting situation is found if more than one discrete state couples to a common continuum. This mutual indirect interaction results in an interference narrowing of the linear line shapes[16] under certain conditions, and we may expect a reduced decay rate of the nonlinear traces. In the frequency domain the coherent dynamics is expressed by the particular features of the linear Fano spectrum. The temporal dynamics seen in the FWM traces reflects these spectral features.

In the present work we want to explore the principal features of FWM traces due to Fano resonances. We will therefore restrict ourselves to the most simple model and ignore the electron-electron interaction altogether. The resonant levels can be thought of as either atomic or molecular states or excitonic resonances in semiconductors. In the latter case the TR traces are strongly modified by many-particle effects.[17] A comparison of the results for, e.g., quantum beats described in terms of the optical Bloch equation on the one hand and in terms of the full many-body dynamical equations[18] on the other hand, however, shows that the dominant features of the dynamics are already obtained without taking into account many-particle effects.[19] For a quantitative description of forthcoming experiments in semiconductors, the application of the many-body semiconductor Bloch equations is, however, mandatory.

We start by introducing the Fano model. The coupling is treated in a phenomenological way, and we do not attempt to explain its microscopical origin for the various possible experimental situations here. The continuum is represented by a dense ensemble of levels. Following the literature[20,21] we diagonalize the excited state part of the Hamiltonian in the presence of the coupling. This leads to an M-level system, where $M \to \infty$. The dipole matrix elements then depend in a characteristic manner on the excitation frequency reflecting the interference between the two concurring optical-excitation paths into resonant levels and into the continuum. The Hamiltonian of the M-level system defines the equation of motion of the density matrix (the optical Bloch equations), from which we calculate the optical polarization. We solve the optical Bloch equations to third order in the laser field and for signals in the phase-matched self-diffraction direction. The TR and TI traces as well as the FWMS are then obtained for various situations.

II. THE MODEL

We start by considering a single level $|a\rangle$ with energy E_a, coupled by an interaction $v_{E_i a}$ to the unstructured continuum states $|\tilde{E}_i\rangle$, see Fig. 1(a). Taking the energy of the ground state to be zero, the Hamiltonian H_0 reads

$$H_0 = E_a|a\rangle\langle a| + \sum_{E_i} E_i|\tilde{E}_i\rangle\langle\tilde{E}_i| + \sum_{E_i}(v_{E_i a}|\tilde{E}_i\rangle\langle a| + \text{H.c.}). \quad (1)$$

The continuum states $|\tilde{E}_i\rangle$ and the state $|a\rangle$ are coupled to the ground state $|g\rangle$ by the light field of two successive pulses,

$$F(t) = F_{01}(t)(e^{i\vec{k}_1\cdot\vec{r}-i\omega_L t} + \text{c.c.}) + F_{02}(t)(e^{i\vec{k}_2\cdot\vec{r}-i\omega_L t} + \text{c.c.}) \quad (2)$$

which are characterized by the envelope functions $F_{01}(t)$ and $F_{02}(t)$. The respective interaction Hamiltonian is

$$H_1 = -F(t)\sum_i(\tilde{v}_{E_i g}|\tilde{E}_i\rangle\langle g| + \text{H.c.}) - F(t)(\tilde{v}_{ag}|a\rangle\langle g| + \text{H.c.}). \quad (3)$$

The optical dipole matrix elements of the discrete level and the continuum states are $\tilde{v}_{ag}$ and $\tilde{v}_{E_i g}$, respectively. Following Refs. 20 and 21, H_0 can be diagonalized neglecting the real part of the self-energy. The new eigenstates $|E_i\rangle$ are coupled to the ground state by the energy-dependent optical matrix elements $\mu(E_i)$,

$$|\mu(E_i)|^2 = \frac{(q+\epsilon)^2}{1+\epsilon^2}\tilde{v}^2_{E_i g} \quad (4)$$

with the Fano parameter

$$q = \frac{\tilde{v}_{ag}}{\pi v_{E_i a}\tilde{v}_{E_i g} g} = \left(\frac{2}{\pi\Gamma g}\right)^{1/2}\frac{\tilde{v}_{ag}}{\tilde{v}_{E_i g}}. \quad (5)$$

Here g is the density of states of the unstructured continuum, Γ is the reciprocal lifetime,

$$\Gamma = 2\pi v_{E_i a}^2 g, \quad (6)$$

and

$$\epsilon = \frac{E - E_a}{\Gamma/2}. \quad (7)$$

Eventually, we will consider more (N) than one single state coupled to the same continuum; see Fig. 1(b) for $N = 2$. Denoting these N discrete levels by $|i\rangle$ and their energies and Fano parameters by E_i and q_i, respectively, we obtain[20,3]

$$|\mu(E)|^2 = \frac{\left(1 + \sum_{i=1}^{N} q_i \frac{\Gamma_i/2}{E - E_i}\right)^2}{1 + \left(\sum_{i=1}^{N} \frac{\Gamma_i/2}{E - E_i}\right)^2} v_0^2. \quad (8)$$

As we will assume an unstructured continuum $|\tilde{E}_i\rangle$ we set $\tilde{v}_{E_i g}^2 = v_0^2$.

In the new basis the Hamiltonian reads

$$H = H_0 - F(t)\cdot\hat{P} \quad (9)$$

with the polarization operator

$$\hat{P} = \sum_{i=1}^{M} \mu(E_i)|E_i\rangle\langle g| + \text{H.c.} \quad (10)$$

and

$$H_0 = \sum_{i=1}^{M} E_i |E_i\rangle\langle E_i|. \quad (11)$$

For this M-level system we set up the equations of motion for the density matrix $\rho_{ij}(t)$, where $\{i,j\} = \{g, E_i\}$. The polarization $P(t)$ is then obtained from

$$P(t) = \mathrm{Tr}(\rho\hat{P}), \quad (12)$$

i.e.,

$$P(t) = \sum_{E_k} \mu(E_k)\rho_{gE_k} + \text{c.c.} \quad (13)$$

The derivation of the equation of motion for the density matrix

$$\dot{\rho} = -i[H(t), \rho] \quad (14)$$

is standard[15] and is given in Appendix A. We will write

$$P(t) = e^{-i\omega_L t}\bar{P}(t) + \text{c.c.} \quad (15)$$

and accordingly

$$\rho_{E_k g}(t) = e^{-i\omega_L t}\bar{\rho}_{E_k g}(t) \quad (16)$$

such that

$$\bar{P}(t) = \sum_{k} \mu^*(E_k)\bar{\rho}_{E_k g}(t). \quad (17)$$

In the rotating wave approximation the equations of motion (the optical Bloch equations) for the resonant contribution $\bar{\rho}(t)$ read

$$\begin{aligned}
\dot{\bar{\rho}}_{E_k g} + i(E_k - \omega_L)\bar{\rho}_{E_k g} &= iF_{0n}(t)e^{i\vec{k}_n\cdot\vec{r}}\mu(E_k)\rho_{gg} - iF_{0n}(t)e^{i\vec{k}_n\cdot\vec{r}}\sum_{E_i}\mu(E_i)\rho_{E_k E_i}, \\
\dot{\rho}_{E_k E_i} + i(E_k - E_i)\rho_{E_k E_i} &= iF_{0n}(t)e^{i\vec{k}_n\cdot\vec{r}}\mu(E_k)\bar{\rho}_{gE_i} - iF_{0n}(t)e^{-i\vec{k}_n\cdot\vec{r}}\mu^*(E_i)\bar{\rho}_{E_k g}, \\
\dot{\rho}_{gg} &= iF_{0n}(t)e^{-i\vec{k}_n\cdot\vec{r}}\sum_{E_k}\mu^*(E_k)\bar{\rho}_{E_k g} - iF_{0n}(t)e^{i\vec{k}_n\cdot\vec{r}}\sum_{E_k}\mu(E_k)\bar{\rho}_{gE_k}.
\end{aligned} \quad (18)$$

This set of optical Bloch equations is the basis of the analytical and numerical calculation discussed below.

III. FOUR-WAVE MIXING

In the self-diffraction geometry of degenerate transient four-wave-mixing experiments (see Fig. 2) a light pulse no. 1 arrives at the sample with wave vector $\vec{k}_1$ at $t = 0$, followed by a delayed (delay time τ) pulse no. 2 with wave vector $\vec{k}_2$. A nonlinear signal is then emitted at times greater than τ in the direction $2\vec{k}_2 - \vec{k}_1$. The signal intensity is proportional to the square of the nonlinear third-order optical polarization $|P^{(3)}(t,\tau)|^2$ of the sample and depends on time t and parametrically on τ. In the time-resolved detection mode (TR) the signal is mixed with a reference pulse in a nonlinear crystal, thus producing a cross-correlation function TR$\propto |P^{(3)}(t,\tau)|^2$, while in the time-integrated mode (TI) the signal is monitored by a slow detector and the output depends on delay τ only, TI $\propto \int_{-\infty}^{\infty} |P^{(3)}(t,\tau)|^2 dt$. The four-wave-mixing spectrum (FWMS) is determined by spectrally resolving the TR signal.

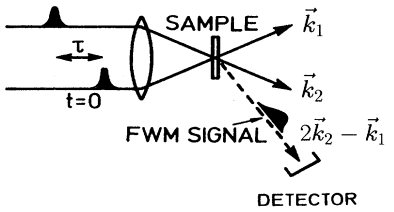

FIG. 2. Schematic drawing of the FWM experiment.

IV. ANALYTICAL SOLUTION FOR δ PULSES

The optical Bloch equations can be solved analytically by assuming ultrashort laser pulses, represented by

$$F_{01} = \eta_1 \delta(t), \qquad (19)$$
$$F_{02} = \eta_2 \delta(t-\tau).$$

Again, the derivation is standard[22] and is given in Appendix B. In linear response to the first pulse the polarization reads

$$\bar{P}^{(1)}(t) = i\eta_1 \Theta(t) e^{i\vec{k}_1\cdot\vec{r}+i\omega_L t} \sum_{E_k} |\mu(E_k)|^2 e^{-iE_k t}. \qquad (20)$$

In third order we obtain for radiation into the self-diffraction direction $2\vec{k}_2 - \vec{k}_1$

$$\bar{P}^{(3)}(t,\tau) = -2i\eta_2 \bar{P}^{(1)}(t-\tau)\bar{P}^{(1)*}(\tau) e^{i\vec{k}_2\cdot\vec{r}}. \qquad (21)$$

Note that within the single-particle picture and for δ-pulse excitation the linear polarization determines the dependence of the third-order polarization on both t and τ.[11] From now on we will omit both the phase factor containing the laser frequency and the spatial phase factors.

V. TRACES AND SPECTRA

We are interested in the time-integrated (TI) traces, the time-resolved (TR) traces, the linear spectrum (LS), and the spectrum of the FWM-signal FWMS, given by

$$\mathrm{TR} \propto |P^{(3)}(t,\tau)|^2, \qquad (22)$$

$$\mathrm{TI} \propto \int_{-\infty}^{\infty} |P^{(3)}(t,\tau)|^2 dt, \qquad (23)$$

$$\mathrm{LS} \propto |\mu(E)|^2, \qquad (24)$$

$$\mathrm{FWMS} \propto \left| \int_{-\infty}^{\infty} P^{(3)}(t,\tau) e^{i\omega t} dt \right|^2. \qquad (25)$$

Since for δ-pulse excitation the nonlinear signal traces and spectra are determined by the linear polarization, we concentrate on this function if analytical results are discussed. For the more general case of finite pulses the full optical Bloch equations are solved numerically. The first-order polarization Eq. (20) can be written as an integral,

$$\bar{P}^{(1)}(t) = i\eta_1 \Theta(t) g \int_{-\infty}^{\infty} e^{-iEt} |\mu(E)|^2 dE \qquad (26)$$

which can be rewritten as

$$\bar{P}^{(1)}(t) = i\eta_1 \Theta(t) g v_0^2 [2\pi\delta(t) + L(t)]. \qquad (27)$$

The absorption into the continuum is represented by the δ-function contribution to the above expression, while the second part $L(t)$ contains the transition into the discrete states and the contribution due to the interference.

VI. SINGLE DISCRETE STATE

We first consider a single state $|a\rangle$ coupled to the continuum and use Eq. (4) which yields

$$L(t) = \pi \frac{\Gamma}{2} (q-i)^2 e^{-iE_a t - \frac{\Gamma}{2}t}. \qquad (28)$$

For $v_0 \to 0$ the optical transitions into the continuum are switched off and the δ contribution vanishes. In this limit we have $g v_0^2 (q-i)^2 \frac{\Gamma}{2}\pi \to \tilde{v}_{ag}^2$, i.e., we obtain the response to a δ pulse of an exponentially damped single absorber corresponding to a Lorentzian linear polarization spectrum.

For $\Gamma \to 0$ we arrive at another trivial limit. Here again $g v_0^2 (q-i)^2 \frac{\Gamma}{2}\pi \to \tilde{v}_{ag}^2$, and the linear polarization is a superposition of the δ contribution due the continuum and a nondecaying signal due to the discrete state.

For $v_0 > 0$, the optical excitation into the continuum interferes with that of the state $|a\rangle$. This interference is described by the term $(q-i)^2$. It is instructive to compare the functions $L(t)$ for the interfering Fano situation and for a noninterfering system described by a Lorentzian line superimposed on a continuum. In the latter case $L(t)$ has the same form as above, except that the term $-i$ is missing. The interference effects are most important for small q values. For large q we get $(q-i)^2 \simeq q^2$, and the Fano line as well as the corresponding FWM traces recover the form characteristic for the non-interfering superposition.

In the case of δ pulses considered above, the term $(q-i)^2$ enters as a prefactor for $t > 0$, and the time dependence of the intensities of both the linear and nonlinear TR signals is completely unaffected by this interference. In view of the nontrivial Fano shape of the linear spectrum this result is rather unexpected. It shows that the TR spectra are signatures of the dynamics and cannot be inferred simply from the linear polarization spectra.

The state $|a\rangle$ influences the optical properties and dynamics of the system even if the transition $|g\rangle \to |a\rangle$ is optically forbidden ($q = 0$). The linear spectrum then shows a Lorentzian hole with zero absorption at E_a due to the admixture of the forbidden transition into the continuum absorption. In the time-dependent signals there

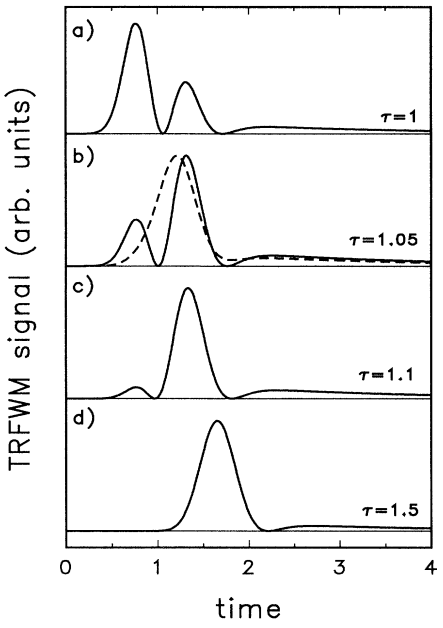

FIG. 3. Time-resolved traces for $N = 1$, $q = 0$, $\Gamma = 0.5$, $\sigma = 0.5$, and various pulse separation τ. The first zero close to $t = 1$ is due to the overlap of the second pulse with the polarization induced by the first pulse. The second zero follows the pulse delay. The dashed line gives the result for $\tau = 1.05$ and $q = 0.5$.

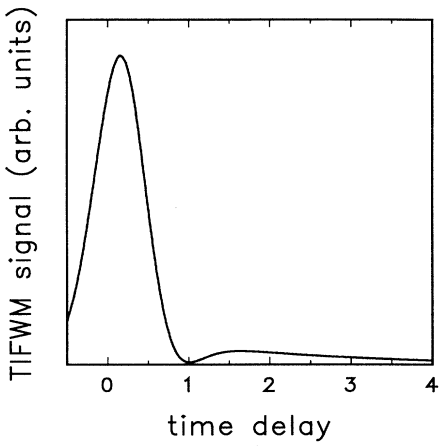

FIG. 4. Time-integrated trace for the parameters of Fig. 3.

is a π-phase shift between the first and second term in Eq. (27). Again, for δ pulses the signal traces remain purely exponential and no effect of this phase shift can be seen in the TR spectra.We therefore expect to see characteristic features in the traces due to interference only if finite pulse widths are considered.

In order to demonstrate this, we have solved the optical Bloch equations (18) numerically for Gaussian pulses $F(t) \propto e^{-t^2/\sigma^2}/\sigma$. For delay times τ sufficiently large to prevent significant pulse overlap, the calculated FWM signal consists of two distinct regimes. At short times the continuum excitation produces a fast decaying structure given by the temporal pulse shape, while at later times the signal is determined by the decay Γ of the function $L(t)$. For $q = 0$ these two regimes are separated by a zero, see Figs. 3(a)–(d), reflecting the π-phase shift due to the interference term $(q-i)^2$. For increasing q the zero converts into a dip [see Fig. 3(b), dashed line] which disappears for large q. This zero or dip in the FWM traces can therefore be seen as a signature of Fano interference. For small τ we obtain an additional zero at shorter times in the FWM traces which is obviously due to the pulse overlap. It is again produced by the π-pulse shift occurring during the arrival of the second pulse.

The TI trace for the set of parameters underlying Fig. 3 is shown in Fig. 4. As pulse overlap effects are integrated over, the TI trace approximately resembles the trace [Fig. 3(d)] for large τ, emphasizing that the TI trace more closely reflects the linear polarization than the TR trace for finite pulse overlap.

VII. TWO DISCRETE STATES

We now consider two states $|a\rangle$ and $|b\rangle$ coupled to the continuum by Γ_a and Γ_b, and with q_a and q_b, respectively. Their energies are E_a and $E_b = E_a + \Delta$. To facilitate the analytical analysis, we choose $\Gamma_a = \Gamma_b = \Gamma$ and $q_a = q_b = q$. This restriction will be relaxed later in our numerical calculations.

The corresponding absorption strength is obtained from Eq. (8). It possesses two poles in the relevant lower complex frequency plane (and two complex conjugate poles in the upper one)

$$E_{1,2} = E_a + \frac{\Delta}{2} \pm \frac{1}{2}\sqrt{\Delta^2 - \Gamma^2} + i\frac{\Gamma}{2}. \tag{29}$$

In the underdamped case ($\Delta > \Gamma$) there are two different frequencies, but only one single damping constant $\Gamma/2$, while in the overdamped case ($\Delta < \Gamma$) a single frequency $E_a + \Delta/2$ exists with two different damping constants. These results correspond to those found in the analysis of population dynamics in double quantum wells coupled to a continuum.[23,24] The linear polarization response to a δ pulse is given by Eq. (27) with

$$L(t) = \frac{\Gamma}{2}\pi(q-i)^2\left(1 - i\frac{\Gamma}{W_1}\right)e^{-i(E_a+\Delta/2+W_1/2)t-(\Gamma/2)t} + (W_1 \to -W_1), \tag{30}$$

$$L(t) = \frac{\Gamma}{2}\pi(q-i)^2\left(1 + \frac{\Gamma}{W_2}\right)e^{-i(E_a+\Delta/2)t-(\Gamma/2+W_2/2)t} + (W_2 \to -W_2), \tag{31}$$

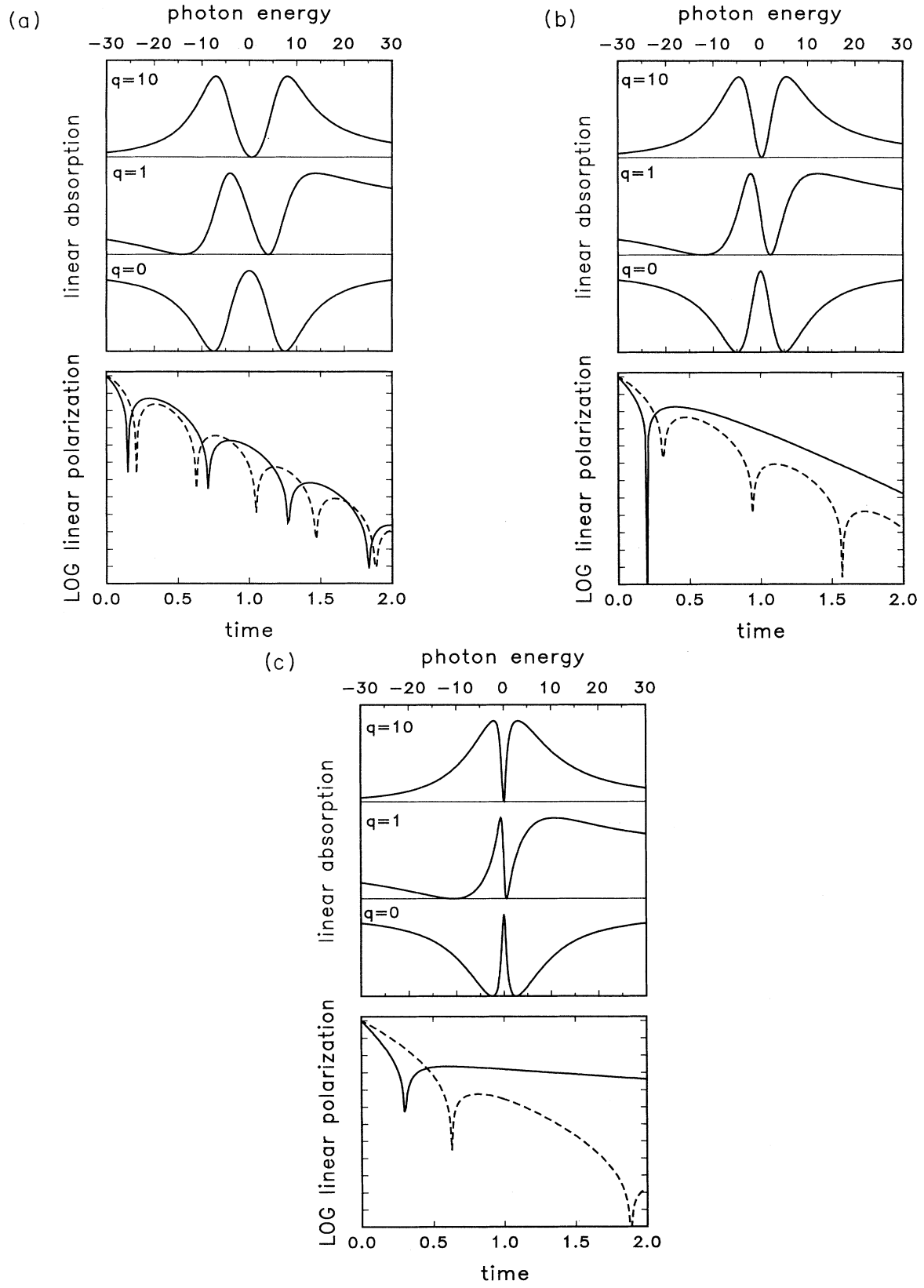

FIG. 5. Linear polarization ($N = 2$) (a) for the underdamped case ($\Delta = 15$, $\Gamma = 10$) showing beats, (b) for the critical case ($\Delta = \Gamma = 10$), and (c) for the overdamped case ($\Delta = 5$, $\Gamma = 10$). The absorption spectra are shown for $q = 10, 1, 0$. Dashed lines correspond to a decay into separate continua.

with real $W_1 = \sqrt{\Delta^2 - \Gamma^2}$ and $W_2 = \sqrt{\Gamma^2 - \Delta^2}$ for the underdamped and the overdamped case, respectively. This result is to be compared with the noninteracting case where the two levels $|a\rangle$ and $|b\rangle$ decay into separate continua (see dashed lines in Fig. 5),

$$L_0(t) = \frac{\Gamma}{2}\pi(q-i)^2(e^{-i(E_a+\Delta)-(\Gamma/2)t} + e^{-iE_at-(\Gamma/2)t}). \tag{32}$$

While in the underdamped case we have damped quantum beats, beating is completely absent in the overdamped situation, see also Fig. 5. At first sight, this looks very surprising, since the linear polarization spectra for both cases look qualitatively similar with their double peak structure, as is shown in Fig. 5 for large q. The absence of quantum beats in the overdamped case can be easily understood by realizing that—in contrast with the underdamped case—the function $|\mu(E)|^2$ is composed from two single-level Fano-like contributions [Eq. (4)] which are centered at the *same* frequency. We note, however, that the overdamped traces are not monotoneous. In fact, there is a single zero in $L(t)$, separating the fast and slow decaying contributions. The phase shift responsible for this can be seen most clearly for $\Gamma/\Delta >> 1$, where

$$L(t) \to -2\frac{\Gamma}{2}\pi(q-i)^2\left(e^{-\Gamma t} - \frac{\Delta^2}{4\Gamma^2}e^{-\frac{\Delta^2}{4\Gamma}t}\right). \tag{33}$$

For short times the first term dominates, while for longer times $L(t)$ is given by the second term which has the opposite sign.

The decaying traces do not depend on the parameter q. This again is rather counterintuitive. In fact, the linear spectra (see Fig. 5, upper part) differ remarkably from each other for different q. The independence of the decaying traces on q is due to the fact that for δ-pulse excitation and for $t > 0$ the q dependence is given by a prefactor, which has no influence on the time dependence. The interference we are discussing here is that between the transitions into the discrete states $|g\rangle \to |a\rangle$ and $|g\rangle \to |b\rangle$, mediated by the common continuum $|\tilde{E}_i\rangle$. Whether or not the continuum is excited as well is of no importance. We will see below that for finite pulse widths this feature is preserved as long as we look at times exceeding the pulse width.

The numerical solution of Eq. (18) can of course be obtained for arbitrary values of the parameters. For short pulses with $\sigma = 0.05$ we recover the analytically obtained results for the same set of parameters.

The π-phase shift separating the fast decaying short-time regime from the slow decaying long-time regime, present for $q_a = q_b$, survives even if finite pulse widths are considered, as shown in Fig. 6 for $\sigma = 0.1$. For large pulse width the zero may convert into a dip, see Fig. 7, which does not look unlike a strongly damped beating signal. However, in this overdamped situation beats are not present.

In atomic (molecular) systems or semiconductor het-

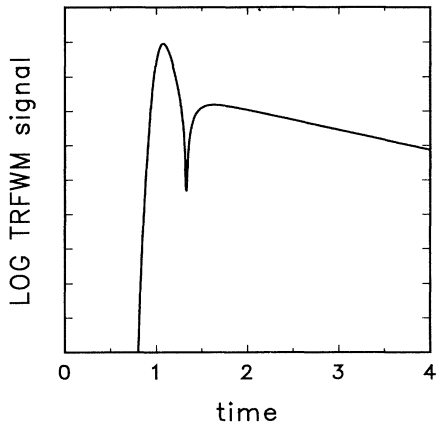

FIG. 6. Time-resolved trace for finite pulse width and for the strongly overdamped case ($N = 2$, $\sigma = 0.1$, $\tau = 1$, $\Delta = 5$, $q_a = q_b = 10$, $\Gamma_a = \Gamma_b = 10$).

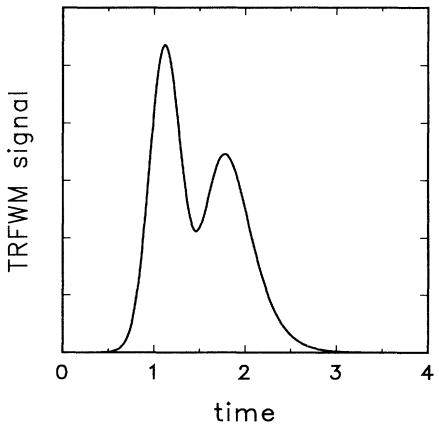

FIG. 7. Pseudobeating for larger pulse width, weakly overdamped case ($N = 2$, $q_a = q_b = 1$, $\Gamma_a = \Gamma_b = 10$, $\Delta = 9$, $\sigma = 0.5$, $\tau = 1$).

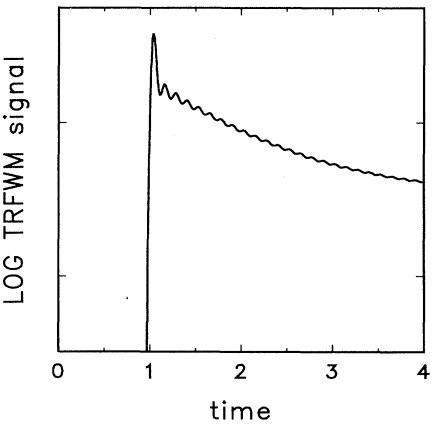

FIG. 8. Time-resolved trace for $N = 2$ and for the overdamped case, one transition being forbidden ($q_a = 0$, $q_b = 10$, $\Gamma_a = \Gamma_b = 0.5$, $\Delta = 0.25$, $\sigma = 0.05$, $\tau = 1$).

erostructures one often encounters the situation in which two successing levels have opposite parity. From the common ground state one of the transitions is then allowed, the other one forbidden. In Fig. 8 we present a TR trace for a pair of discrete levels with finite q_a and $q_b = 0$ for the overdamped case. Now the fast and slow components are no longer separated by a zero, even for the short pulse width of $\sigma = 0.05$ assumed here. (The high frequency wiggles are due to the high- and low-energy boundaries used in the numerical description of the continuum.)

VIII. THE FOUR-WAVE-MIXING SPECTRUM

For δ-pulse excitation we are again able to calculate the FWMS [see Eq. (25)] analytically. From Eq. (21) we have

$$\text{FWMS} \propto \left| \int_0^\infty \bar{P}^{(1)}(t) e^{i\omega t} dt \right|^2 . \tag{34}$$

For δ-pulse excitation the linear polarization is essentially the linear optical susceptibility, $\bar{P}^{(1)}(t) = \eta\chi(t)$, and therefore

$$\text{FWMS} \propto \chi'^2(\omega) + \chi''^2(\omega), \tag{35}$$

where

$$\chi(\omega^+) = \frac{1}{\pi} \int_0^\infty \chi(t) e^{i\omega^+ t} dt = \chi'(\omega) + i\chi''(\omega) \tag{36}$$

is the complex linear response function, which for δ-pulse excitation reads

$$\chi(\omega) = igv_0^2 \left(1 + \frac{1}{\pi} \int_0^\infty L(t) e^{i\omega t} dt \right). \tag{37}$$

The dissipative part is the linear optical absorption spectrum, $\chi''(\omega) = gv_0^2 |\mu(E)|^2$, and the reactive part its Kramers-Kronig transform,

$$\chi'(\omega) = \mathcal{P} \frac{d\omega}{\pi} \frac{\chi''(\omega')}{\omega' - \omega}. \tag{38}$$

For one single discrete state we obtain

$$\chi(\omega) = igv_0^2 \left(1 + \frac{\frac{\Gamma}{2}(q-i)^2}{\frac{\Gamma}{2} - i(\omega - E_a)} \right) \tag{39}$$

and

$$\text{FWMS} \propto (gv_0^2)^2 \frac{q^4 + 4q^2 + 4q\epsilon + \epsilon^2}{1 + \epsilon^2}. \tag{40}$$

An example is shown in Fig. 9. The asymmetry of the linear Fano-absorption spectrum is still present, but the zero is suppressed by the contribution of the reactive susceptibility $\chi'(\omega)$ to the FWMS.

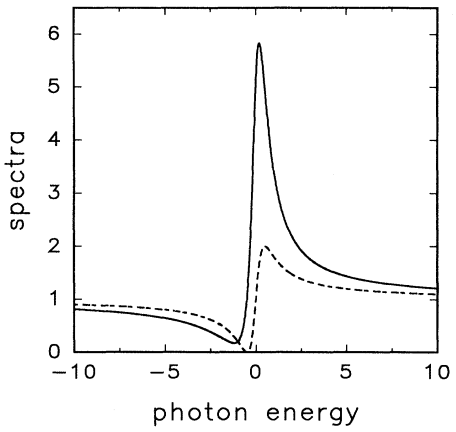

FIG. 9. Linear absorption spectrum (dashed line) and FWM spectrum (solid line) for $N = 1$, $q = -1$, $\Gamma = 1$.

IX. CONCLUSIONS

In the present work we have looked for characteristic features in the FWM traces, which can be used to identify Fano interaction. Our results show that in systems with a single discrete state coupled to a continuum, the identification of a Fano interference in terms of FWM traces is possible if the oscillator strength for the discrete transition is weaker than that of the continuum. In this case a single dip, or even zero (for forbidden discrete transitions) is predicted in both the time-integrated and time-resolved traces, provided the pulse separation is sufficiently large. For overlapping pulses an additional dip is produced in the temporal range of overlap. The interference features become negligible if the transition probability into the discrete level becomes large with respect to the transition probability into the continuum, and the traces recover the form of those produced by a simple superposition of a damped resonance and a continuum.

For two discrete states coupled to a continuum with strength Γ and separated by an energy ΔE, one has to distinguish between the underdamped ($\Delta E > \Gamma$) and the overdamped case ($\Delta E < \Gamma$). Beats are seen in the underdamped situation, determined by the separation of the broadened spectral peaks. Quite surprisingly, although the linear polarization spectrum of the overdamped case looks very similar and also shows two peaks, there are no beats in the corresponding FWM traces. Instead, a fast initial component followed by a slow component at later times is predicted. This feature can be seen as the time analog of Fano-interference narrowing. For equal optical transition probabilities into the two discrete states, the fast and slow components are separated by a zero in TR traces. This zero disappears if the transition probabilities are different. The effects due to interference of two states, mediated by a common continuum, are seen irrespective of the strength of the absorption into the continuum.

The signatures of interference in the temporal traces express the particular form of the energy dependence of

the dipole matrix elements. Spectra resulting from a simple superposition of peaks, although looking similar to a Fano line, will not produce the features discussed here. Therefore, it would be extremely interesting to look for these interference phenomena in FWM experiments performed on atomic or molecular systems. Similar measurements could also be performed for semiconductor heterostructures. In this case one has the additional possibility to design the band structure and thus the excitonic level scheme at will. It should, however, be noted that the many-particle Coulomb interaction in semiconductors is expected to have a strong influence on the TR-FWM traces. Further theoretical work is therefore needed to substantiate the predictions drawn here in this case.

ACKNOWLEDGMENTS

For stimulating discussions we would like to thank G. von Plessen, U. Siegner, and S.W. Koch. This work has been supported in part by the Deutsche Forschungsgemeinschaft.

APPENDIX A

Taking matrix elements of the equation of motion (14) we obtain

$$\begin{aligned} i\dot{\rho}_{gE_k} &= \sum_{E_n}\langle g|H|E_n\rangle\rho_{E_nE_k} \\ &\quad - \sum_{E_n}\rho_{gE_n}\langle E_n|H|E_k\rangle - \rho_{gg}\langle g|H|E_k\rangle \qquad \text{(A1)} \\ &= -E_k\rho_{gE_k} + F(t)\mu^*(E_k)\rho_{gg} \\ &\quad -F(t)\sum_{E_i}\mu^*(E_i)\rho_{E_iE_k} \end{aligned}$$

and

$$\begin{aligned} i\dot{\rho}_{gg} &= \sum_{E_k}\langle g|H|E_k\rangle\rho_{E_kg} - \sum_{E_k}\rho_{gE_k}\langle E_k|H|g\rangle \qquad \text{(A2)} \\ &= -F(t)\sum_{E_k}\mu^*(E_k)\rho_{E_kg} - F(t)\sum_{E_k}\mu(E_k)\rho_{gE_k}, \end{aligned}$$

$$\begin{aligned} i\dot{\rho}_{E_kE_i} &= \langle E_k|H|g\rangle\rho_{gE_i} - \rho_{E_kg}\langle g|H|E_i\rangle \\ &\quad + \sum_{E_j}\langle E_k|H|E_j\rangle\rho_{E_jE_i} - \sum_{E_j}\rho_{E_kE_j}\langle E_j|H|E_i\rangle \qquad \text{(A3)} \\ &= (E_k - E_i)\rho_{E_kE_i} - F(t)\mu(E_k)\rho_{gE_i} \\ &\quad + F(t)\mu^*(E_i)\rho_{E_kg}. \end{aligned}$$

The set of equations then reads

$$\begin{aligned} \dot{\rho}_{E_kg} + iE_k\rho_{E_kg} &= iF(t)\mu(E_k)\rho_{gg} \\ &\quad -iF(t)\sum_{E_i}\mu(E_i)\rho_{E_kE_i}, \\ \dot{\rho}_{E_kE_i} + i(E_k - E_i)\rho_{E_kE_i} &= iF(t)\mu(E_k)\rho_{gE_i} \qquad \text{(A4)} \\ &\quad -iF(t)\mu(E_i)^*\rho_{E_kg}, \\ \dot{\rho}_{gg} &= iF(t)\sum_{E_k}\mu^*(E_k)\rho_{E_kg} \\ &\quad -iF(t)\sum_{E_k}\mu(E_k)\rho_{gE_k}. \end{aligned}$$

With

$$\rho_{E_kg}(t) = e^{-i\omega_L t}\bar{\rho}_{E_kg}(t) \qquad \text{(A5)}$$

we have

$$\begin{aligned} [\dot{\bar{\rho}}_{E_kg} + i(E_k - \omega_L)\bar{\rho}_{E_kg}]e^{-i\omega_L t} &= iF(t)\mu(E_k)\rho_{gg} - iF(t)\sum_{E_i}\mu(E_i)\rho_{E_kE_i}, \qquad \text{(A6)} \\ \dot{\rho}_{E_kE_i} + i(E_k - E_i)\rho_{E_kE_i} &= iF(t)\mu(E_k)\bar{\rho}_{gE_i}e^{i\omega_L t} - iF(t)\mu^*(E_i)\bar{\rho}_{E_kg}e^{-i\omega_L t}, \\ \dot{\rho}_{gg} &= iF(t)\sum_{E_k}\mu^*(E_k)\bar{\rho}_{E_kg}e^{-i\omega_L t} - iF(t)\sum_{E_k}\mu(E_k)\bar{\rho}_{gE_k}e^{i\omega_L t}. \end{aligned}$$

We insert $F(t)$, apply the rotating wave approximation by omitting all nonresonant terms, and finally obtain Eq. (18).

APPENDIX B

In linear response (i.e., with $\rho_{gg} = 1$ and $\rho_{E_kE_i} = 0$) to the first pulse Eq. (18) reduces to

$$\dot{\bar{\rho}}_{E_kg} + i(E_k - \omega_L)\bar{\rho}_{E_kg} = i\eta_1\delta(t)\mu(E_k)e^{i\vec{k}_1\cdot\vec{r}} \qquad \text{(B1)}$$

which is solved by

$$\bar{\rho}^{(1)}_{E_kg} = i\mu(E_k)\eta_1 e^{-i(E_k-\omega_L)t}\Theta(t)e^{i\vec{k}_1\cdot\vec{r}}, \qquad \text{(B2)}$$

i.e.,

$$\bar{P}^{(1)}(t) = i\eta_1\Theta(t)e^{i\vec{k}_1\cdot\vec{r}+i\omega_L t}\sum_{E_k}|\mu(E_k)|^2e^{-iE_kt}. \qquad \text{(B3)}$$

In second order (first pulse no. 1, second pulse no. 2) we obtain

$$\begin{aligned} &\dot{\rho}_{E_kE_i} + i(E_k - E_i)\rho_{E_kE_i} \\ &\qquad = i\eta_2\delta(t-\tau)\mu(E_k)\bar{\rho}^*_{E_ig}(\tau)e^{i\vec{k}_2\cdot\vec{r}} \qquad \text{(B4)} \end{aligned}$$

which in turn is solved by

$$\rho^{(2)}_{E_k E_i} = i\eta_2 \Theta(t-\tau)\bar{\rho}^{(1)*}_{E_i g}(\tau) e^{-i(E_k - E_i)(t-\tau)} \mu(E_k) e^{i\vec{k}_2 \cdot \vec{r}} \tag{B5}$$

and analogously

$$\rho^{(2)}_{gg} = -i\eta_2 \Theta(t-\tau) \sum_{E_k} \mu(E_k) \bar{\rho}^{(1)*}_{E_k g}(\tau) e^{i\vec{k}_2 \cdot \vec{r}}. \tag{B6}$$

Finally, in third order (first pulse no. 1, then twice the pulse no. 2) the equation of motion for $\bar{\rho}^{(3)}_{E_k g}$, giving the third-order polarization, reads

$$\begin{aligned} \dot{\bar{\rho}}^{(3)}_{E_k g} + i(E_k - \omega_L)\bar{\rho}_{E_k g} = {} & i\eta_2 \delta(t-\tau)\mu(E_k)\rho^{(2)}_{gg}(\tau) e^{i\vec{k}_2 \cdot \vec{r}} \\ & -i\eta_2 \delta(t-\tau) \\ & \times \sum_{E_i} \mu(E_i) \rho^{(2)}_{E_k E_i}(\tau) e^{i\vec{k}_2 \cdot \vec{r}} \end{aligned} \tag{B7}$$

with the solution

$$\begin{aligned} \bar{\rho}^{(3)}_{E_k g} = {} & 2\eta_2^2 \Theta(t-\tau) e^{-i(E_k - \omega_L)(t-\tau)} \mu(E_k) \\ & \times \sum_{E_i} \mu(E_i) \bar{\rho}^{(1)*}_{E_i g}(\tau) e^{2i\vec{k}_2 \cdot \vec{r}} \end{aligned} \tag{B8}$$

which corresponds to radiation into the direction $2\vec{k}_2 - \vec{k}_1$. There are other terms, which we omit, radiating into different directions. The polarization to third order is then given by Eq. (21).

[1] S. Glutsch, U. Siegner, M.-A. Mycek, and D.S. Chemla, Phys. Rev. B **50**, 17 009 (1994).
[2] D.Y. Oberli, G. Böhm, G. Weimann, and J.A. Brum, Phys. Rev. B **49**, 5757 (1994).
[3] K. Maschke, P. Thomas, and E.O. Göbel, Phys. Rev. Lett. **67**, 2646 (1991).
[4] D.A. Broido, E.S. Koteles, C. Jagannath, and J.Y. Chi, Phys. Rev. B **37**, 2725 (1988); D.A. Broido and L.J. Sham, *ibid.* **34**, 3917 (1986).
[5] H. Chu and Y.-C. Chang, Phys. Rev. B **39**, 10 861 (1989)
[6] G. von Plessen, J. Feldmann, E.O. Göbel, K. Goossen, D.A.B. Miller, and J.E. Cunningham, Appl. Phys. Lett. **36**, 2372 (1993).
[7] J.J. Hopfield, P.J. Dean, and D.J. Thomas, Phys. Rev. **158**, 748 (1967).
[8] D.S. Chemla, A. Maruani, and E. Batifol, Phys. Rev. Lett. **42**, 1075 (1979).
[9] F. Cerdaira, T.A. Fjeldly, and M. Cardona, Phys. Rev. B **8**, 4734 (1973); M. Chandrasekhar, J.B. Renucci, and M. Cardona, *ibid.* **17**, 1623 (1978); K.-J. Jin, Sh.-H. Pan, and G.-Zh. Yang, *ibid.* **50**, 8584 (1994).
[10] M.D. Sturge, Phys. Rev. **127**, 768 (1962); M.V. Kurik, Phys. Status Solidi A **8**, 9 (1971).
[11] M. Koch, J. Feldmann, G. von Plessen, E.O. Göbel, and P. Thomas, Phys. Rev. Lett. **69**, 3631 (1992).
[12] M. Lindberg, R. Binder, and S.W. Koch, Phys. Rev. A **45**, 1865 (1992).
[13] D. Bennhardt, P. Thomas, R. Eccleston, E.J. Mayer, and J. Kuhl, Phys. Rev. B **47**, 13 485 (1993).
[14] J. Feldmann, T. Meier, G. von Plessen, M. Koch, E.O. Göbel, P. Thomas, G. Bacher, C. Hartmann, H. Schweizer, W. Schäfer, and H. Nickel, Phys. Rev. Lett. **70**, 3027 (1993).
[15] K. Leo, J. Shah, T.C. Damen, A. Schulze, T. Meier, S. Schmitt-Rink, P. Thomas, E.O. Göbel, Sh.L. Chuang, M.S.C. Luo, W. Schäfer, K. Köhler, and P. Ganser, IEEE J. Quantum Electron. **28**, 2498 (1992).
[16] F.H. Mies, Phys. Rev. **175**, 164 (1968).
[17] M. Wegener, D.S. Chemla, S. Schmitt-Rink, and W. Schäfer, Phys. Rev. A **42**, 5675 (1990).
[18] H. Haug and S.W. Koch, *Quantum Theory of the Optical and Electronic Properties of Semiconductors*, 3rd ed. (World Scientific, Singapore, 1994).
[19] F. Jahnke, M. Koch, T. Meier, J. Feldmann, W. Schäfer, P. Thomas, S.W. Koch, E.O. Göbel, and H. Nickel, Phys. Rev. B **50**, 8114 (1994).
[20] U. Fano, Phys. Rev. **124**, 1866 (1961).
[21] G.S. Agarwal, S.C. Haan, and J. Cooper, Phys. Rev. A **29**, 2552 (1984).
[22] L.Q. Lambert, A. Compaan, and I.D. Abella, Phys. Rev. A **4**, 2022 (1971).
[23] S.A. Gurvitz, I. Bar-Joseph, and B. Deveaud, Phys. Rev. B **43**, 14 703 (1991).
[24] H. Vaupel, Ph.D. thesis, University of Marburg, 1994.